Available online at www.sciencedirect.com
SCIENCE DIRECT®
Journal of Sound and Vibration 281 (2005) 593–609
JOURNAL OF SOUND AND VIBRATION
www.elsevier.com/locate/jsvi

On the dynamic properties of axially moving systems

Francesco Pellicano*

Dipartimento di Ingegneria Meccanica e Civile, Università di Modena e Reggio Emilia, V. Vignolese, 905, I-41100 Modena, Italy

Received 30 June 2003; accepted 27 January 2004
Available online 5 November 2004

Abstract

The objective of the present paper is a deep analysis of some recent numerical and experimental results regarding the complex dynamics of axially moving systems. Such important mechanical systems exhibit interesting dynamic behaviors: homoclinic orbits; sub-harmonic responses; amplitude modulations; and chaos. These dynamics have been obtained numerically and in some cases have been experimentally observed.

Using recent techniques of the non-linear time series analysis, the response of axially moving systems has been studied for a large variety of test cases. The correlation dimension of the time series, which is deeply related to the minimal dimension of a system able to reproduce the dynamics, is estimated. Lyapunov exponents are evaluated in order to quantify the response regularity.

The present work gives a contribution towards understanding the complex dynamics observed both in conservative and dissipative systems. The dynamical phenomena are analyzed within the unified framework of the non-linear time series analysis.

In the case of experimental data the new non-linear filtering techniques, based on the embedding techniques, have been applied to reduce high noise when classical techniques give bad results.

1. Introduction

In many industrial processes slender translating elements are used for transmitting power, information, and material; these elements are classified as axially moving systems. Chain and belt

*Tel.: +39-059-205-6154; fax: +39-059-205-6129.
E-mail address: frank@unimore.it (F. Pellicano).

0022-460X/$ - see front matter © 2004 Elsevier Ltd. All rights reserved.
doi:10.1016/j.jsv.2004.01.029

drives, magnetic tapes, band saws, packaging, paper-handling machineries are some examples where transverse vibrations occur together with an axial transport of mass.

The first works regarding axially moving systems appeared in the middle of the previous century and were motivated by instability phenomena observed in oil pipelines [1]. In Ref. [2], the effect of the axial velocity on the linear frequencies of moving threadlines was qualitatively discussed; in Ref. [3] the role of non-linearities and axial speed in traveling strings was investigated. Naguleswaran and Williams [4] considered the parametric excitation of band saw systems due to the axial tension fluctuation. They observed violent vibrations when the parametric resonance was subharmonic (2:1), and performed a perturbation analysis with experimental validations. Mockensturm et al. [5] analyzed axially moving continua considering the parametric excitation due to non-trivial boundary conditions in the axial displacement; limit cycles in the speed range close to parametric resonances were found. An experimental investigation of direct and parametric excitation of a belt, and non-linear parametric identification is present in Ref. [6]. Shih [7] presented a three-dimensional vibrational model of a travelling string analyzing the hyperbolicity of the governing equations and the singularities occurring at the critical speed; in that work the elliptic ballooning was analyzed, confirming the experimental results of Ames et al. [8]. In Ref. [9] an energy approach, in Eulerian coordinates, was used to write down the governing equations; the eigenfunctions were obtained through the solution of the dispersion equation. In Ref. [10] orthogonality conditions for complex modes were given; some stability regions also were found in the super-critical speed range, i.e., for specific intervals of the super-critical speed range the trivial equilibrium position regains stability.

Holmes [11] showed that systems governed by the equation of damped axially moving beams with fixed ends can exhibit only pitchfork-like instabilities. Païdoussis and Moon [12] studied, both analytically and experimentally, flutter and chaos in a cantilever pipe. This problem does not belong to the class analyzed by Holmes [11], who restricted his analysis to systems fixed at both ends.

Wickert [13] studied non-linear vibrations and bifurcations of moving beams. He examined the sub- and super-critical speed ranges, performing a local analysis to study small-amplitude non-linear oscillations close to the unstable trivial position and the stable bifurcated positions. The existence of a global motion around the critical speed was predicted by using an asymptotic analysis. A detailed analysis of bifurcation and stability was performed in Refs. [14,15], where the perturbing effect of the beam curvature at the pulleys was accounted for. In Refs. [16,17] the supercritical speed range was analyzed using a high-dimensional discrete model obtained by the Galerkin procedure. Further analyses on the stability of parametrically excited axially moving systems are presented in Ref. [18].

Lin [19] studied the linear vibrations of travelling plates; beam and string theories were compared with plate theory: the beam model overestimates and string model underestimates the critical speed. Moreover, it was found that, in the super-critical speed range, the trivial equilibrium position is always unstable. Such results highlight the main discrepancies between plates and beam/string theories, which are particularly important for small width–length ratios and high flexural stiffness.

In this paper the recent results presented in Refs. [6,16–18] regarding regular and chaotic response of axially moving systems are reanalyzed, in order to clarify the dynamic character of the response. The recent numerical and experimental investigation on this subject evidenced that a wide class of non-linear phenomena can take place, for example: homoclinic orbits; sub-harmonic responses; amplitude modulations; and chaos.

In the past, both analytical techniques and numerical models have been used to reproduce or forecast experimental observations. Usually analytical modelling is performed by means of a minimal number of degrees of freedom; conversely, in the numerical modelling a large number of degrees of freedom are used. Nevertheless, in some cases, chaotic dynamics, analyzed by means a large number of degrees of freedom (d.o.f.), presented a scenario surprisingly similar to that of a chaotic 1-d.o.f. Duffing oscillator, even though convergence tests proved that, using a certain basis, a large number of degrees of freedom is mandatory. Moreover, the comparison between modelling and experiments showed that some dynamical behaviors observed in the experiments were lost in the numerical simulations.

In order to furnish a contribution toward the final answer to the previously mentioned questions, in this paper, after a short theoretical introduction, which also contains some new development regarding the Hamiltonian character of the equations of motion, a systematic analysis of the most interesting dynamics is provided.

The idea is to extract some useful information regarding the dynamical behavior of the system from simulated or experimental data. The approach followed in the analysis is the same for numerical and experimental data: experimental data have been obtained by measuring the mi-span oscillation of the belt using a Laser telemeter; numerical data have been obtained by simulating a measurement on the same position.

Using non-linear time series analysis [20–29] a statistical evaluation of the dimension of the attractor where the system evolves is made. Such dimension gives information about the minimal dimension of a model able to reproduce the dynamics analyzed; it is of fundamental importance when low-dimensional models are developed: their dimension cannot be smaller than the minimal one [22]. Moreover, the maximum Lyapunov exponent has been estimated in order to check the sensitivity to perturbation of the initial conditions.

Non-linear time series methods have also been used for reducing noise in strongly polluted data, on which no classical noise reduction methods were able to reduce the noise sufficiently. The non-linear filter used in this work is a quite new technique and is based on embedding techniques.

2. Governing equations

In this section an analytical model used in the past [6,16–18] to simulate the non-linear response of a power transmission belt is considered. The governing equations are developed on the basis of the system represented in Fig. 1, which is useful to simulate some experiments performed on a belt pulley system with a fixed tensioner and an eccentric pulley. In Fig. 1 the spring, located at the right end, simulates the effect of the lower belt span, considering the longitudinal elasticity but neglecting the lower span dynamics.

The governing equation is [6,16–18]:

$$\begin{aligned} &EI\tilde{w}^{\mathrm{IV}} + \rho A\ddot{\tilde{w}}(\tilde{x},\tilde{t}) + 2\rho A\tilde{v}\dot{\tilde{w}}'(\tilde{x},\tilde{t}) + \rho A\tilde{v}^2\tilde{w}''(\tilde{x},\tilde{t}) - \tilde{P}\tilde{w}''(\tilde{x},\tilde{t}) \\ &\quad - EA\tilde{w}''(\tilde{x},\tilde{t})\left[\frac{1}{2}\frac{K}{Kl+EA}\int_0^{\ell}\tilde{w}'^2(\tilde{x},\tilde{t})\,\mathrm{d}\tilde{x} + \frac{1}{2}\frac{EA}{Kl+EA}\tilde{w}'^2(l,\tilde{t})\right] = \tilde{f}(\tilde{x},\tilde{t}), \end{aligned} \tag{1}$$

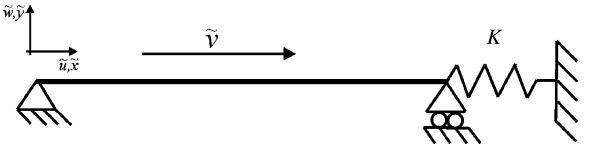

Fig. 1. Physical model of the travelling beam.

where $(\cdot)' = \partial(\cdot)/\partial\tilde{x}$, $\dot{(\cdot)} = \partial(\cdot)/\partial\tilde{t}$, E is Young's modulus, I is the moment of inertia of the cross-section area, ρ is the mass density, A is the cross-section area, $\tilde{w}$ is the transversal displacement field, $\tilde{v}$ is the axial speed, $\tilde{P}(\tilde{t})$ is the time-dependent tension, $\tilde{f}$ is an external excitation field acting directly on the belt, l is the distance between supports, $\tilde{x}$ is the axial coordinate, $\tilde{t}$ is the time, $\tilde{w}_0(\tilde{t})$ is the left support motion (the pulley eccentricity), and K is the spring constant.

The following boundary conditions are considered:

$$\tilde{w}(0,\tilde{t}) = \tilde{w}_0(\tilde{t}), \quad \tilde{w}(l,\tilde{t}) = 0, \tag{2a}$$

$$\tilde{w}''(0,\tilde{t}) = \tilde{w}''(l,\tilde{t}) = 0. \tag{2b}$$

In Ref. [18] the tension fluctuation was due to the pulley eccentricity: $\tilde{P} = P - \tilde{p}(\tilde{t})$, $\tilde{p}(\tilde{t}) = \bar{p}\,\sin(\varphi(\tilde{t})) = \bar{p}\,\sin(\tilde{\omega}\tilde{t})$; similarly, $\tilde{w}_0(\tilde{t}) = \bar{w}_0\cos(\tilde{\omega}\tilde{t})$; where: $\tilde{\omega} = \tilde{v}/R$ [rad/s] was the motor rotation speed and R the pulley radius. The tension fluctuation and the seismic excitations can also be due to other kind of disturbances; for example in Ref. [17] the distributed force filed $\tilde{f}$ was an external point excitation. Therefore, Eq. (1) can be useful for studying a large class of axially moving systems.

A non-dimensional form of Eq. (1) can be obtained by introducing the following variables and parameters: $\hat{w} = \tilde{w}/l$, $x = \tilde{x}/l$, $t = \tilde{t}\sqrt{P/\rho A l^2}$, $v = \tilde{v}/\sqrt{P/\rho A}$, $v_f = \sqrt{EI/Pl^2}$, $p = \tilde{p}/P$. Moreover, the boundary conditions (2a) can be transformed into homogeneous boundary conditions, without loss of generality, by using a new variable

$$\hat{w}(x,t) = w(x,t) + (1-x)w_0(t), \tag{3}$$

where $w_0 = \tilde{w}_0/l$. The resulting non-dimensional equation becomes

$$\begin{aligned} &v_f^2 w^{\mathrm{IV}}(x,t) + \ddot{w}(x,t) + 2v\dot{w}'(x,t) + (v^2 - 1 + p(t))w''(x,t) - 2v\dot{w}_0(t) + (1-x)\ddot{w}_0(t) \\ &\quad - \frac{EA}{P}w''(x,t)\left[\frac{1}{2}\frac{Kl}{Kl+EA}\int_0^1 (w'^2(x,t) - 2w_0(t)w'(x,t) + w_0^2(t))\,\mathrm{d}x\right. \\ &\quad \left. + \frac{1}{2}\frac{EA}{Kl+EA}(w'^2(1,t) - 2w_0(t)w'(1,t) + w_0^2(t))\right] = f(x,t). \end{aligned} \tag{4}$$

The following non-dimensional parameters are introduced: $v_1 = \sqrt{\frac{1}{2}EA\,Kl/(P(Kl+EA))}$ and $v_2 = \sqrt{\frac{1}{2}(EA)^2/(P(Kl+EA))}$. In the experiments it was found that $w_0 \ll 1$ and $w < 1$; therefore,

the terms $w''(x,t)v_1^2\int_0^1(-2w_0(t)w'(x,t)+w_0^2(t))\,dx$ and $w''(x,t)v_2^2(-2w_0(t)w'(1,t)+w_0^2(t))$ can be neglected.

The terms $2v(\partial^2 w/\partial x\partial t)$ and $v^2(\partial^2 w/\partial x^2)$ are the Coriolis force and the centrifugal force, respectively, while the remaining inertial and elastic terms are well known in beam-string theory.

The dynamics of axially moving systems are greatly affected by the axial speed, in particular, the straight equilibrium configuration may lose stability and multiple equilibrium positions may arise when the axial speed increases beyond a critical value, which depends on the flexural stiffness and the initial tension. When external excitations cause resonances a complex dynamic behavior can be encountered: sub-harmonic responses, amplitude modulations, chaotic dynamics and intermittency.

Bifurcations of the fixed point of Eq. (1) arise when the axial speed reaches the critical values: $v^{(m)}=\sqrt{1+(m\pi v_f)^2}$, $m=1,2,\ldots,\infty$; the corresponding non-trivial fixed points are $w_m=\pm 2/m\pi v_T\sqrt{v^2-v^{(m)^2}}\sin m\pi x$, $m=1,2,\ldots,\infty$, where $v_T=\sqrt{EA/P}$ [13,16,30]. After the first critical speed $v^{(1)}$, the straight configuration loses stability; for higher speed, this configuration could regain stability due to the stabilizing effect of the Coriolis forces [13,16].

3. Discretized model and Hamiltonian properties

In order to perform a numerical analysis of Eq. (4), the displacement field is expanded by means of a complete set of functions, which respect the homogeneous boundary conditions. In Refs. [16–18] the following series showed good convergence properties:

$$w(x,t)=\sum_{n=1}^{N} q_n(t)\sin\ n\pi x, \tag{5}$$

where N depends on the smoothness of the displacement field $w(x,t)$ [16]. The Galerkin method is applied, the operator given by Eq. (4) is projected on basis (5), and a finite-dimensional dynamical system is obtained

$$\ddot{\mathbf{q}}+\mathbf{C}\dot{\mathbf{q}}+\mathbf{K}(t)\mathbf{q}=\mathbf{N}(\mathbf{q},\mathbf{t}), \tag{6}$$

where $\mathbf{C}$ is the gyroscopic matrix, and $\mathbf{K}$ is the stiffness matrix, which is time variant due to the presence of $p(t)$ in Eq. (4), and $\mathbf{N}(\mathbf{q},t)$ collects the non-linearities and the direct excitation, $w_0(t)$.

It can be proven that system (6) is Hamiltonian when no damping and forcing are present, see the Appendix; a first integral for system (6) is

$$H(\dot{\mathbf{q}},\mathbf{q})=\tfrac{1}{2}\dot{\mathbf{q}}^{\mathrm{T}}\dot{\mathbf{q}}+U(\mathbf{q}), \tag{7}$$

where

$$U(\mathbf{q})=\frac{1}{2}\sum_{n=1}^{N}K_n q_n^2+\frac{1}{4}\sum_{n=1}^{N}\sum_{k=1}^{N}\beta_{nk}q_n^2q_k^2. \tag{8}$$

The Hamiltonian function (7) is constant; it can be adopted to check the accuracy of the numerical algorithms used to integrate high-dimensional dynamical systems. In particular, it will

be proven that the solution of Eq. (6) can show a chaotic behavior maintaining the property given by Eq. (7). Tests on the Hamiltonian function are particularly important; indeed, Hamiltonian systems are always on the stability bounds, i.e., the eigenvalues of the linearized systems are purely imaginary. The latter feature is extremely dangerous for numerical integration algorithms such as Runge–Kutta methods, which are not generally energy preserving. When the dynamics becomes complex, for example in chaotic dynamics, some doubt can arise on the origin of instability of regular motion. The Hamiltonian function test gives a proof of the quality of integration.

4. Time series analysis: embedding techniques, noise filtering, correlation dimension and Lyapunov exponents

In order to analyze chaotic time histories, an estimation of the phase space dimension where the system evolves could be useful along with the evaluation of the maximum Lyapunov exponent. The correlation dimension gives an estimate of the number of degrees of freedom needed to model the observed dynamics. The maximum Lyapunov exponent indicates if an exponential divergence from the initial conditions is present, i.e., indicates when a chaotic motion takes place.

In the case of a highly polluted system the direct estimation of the previously mentioned statistical indicators may be impossible; in these cases noise filtering techniques can be useful to reduce noise and improve the estimations.

In the present section the correlation dimension, the maximum Lyapunov exponent and data-filtering algorithms are briefly described. The TISEAN software is used in this work; a full description of such algorithms can be found in Refs. [29,33].

4.1. Embedding techniques

When a single time history is available, for example from a single measurement, an image of the actual phase space can be reconstructed using embedding techniques [31]: let us suppose that the time history $w(\hat{x},t)$ is sampled, the time series is: $w_i = w(\hat{x}, i \times \Delta t)$, where Δt is the sampling interval and $i = 1,\ldots,N_T$. A delay coordinate vector can be defined as follows: $\mathbf{v}_i = \{w_{i-(M-1)d}, w_{i-(M-2)d}, \ldots, w_i\}$, $i = (M-1)\times d,\ldots,N_T$; $d\cdot\Delta t$ is called time delay, M is the embedding dimension. The embedding theorem [31] states that if the time series consists of scalar measurements of a dynamical system and M is large enough, then the time delay embedding provides a one-to-one image of the original phase space.

4.2. Correlation dimension

The correlation integral [20,21] is given by

$$C(r) = \frac{1}{N_{\text{pairs}}} \sum_{i=M}^{N_T} \sum_{j<i-k} H\big(r - ||\mathbf{v}_i - \mathbf{v}_j||\big), \tag{9}$$

where $N_{\text{pairs}} = \frac{1}{2}(N_T - M + 1)\times(N_T - M - k + 1)$, r is a scalar length scale, k is related to the Theiler window [32], and H is the Heaviside function.

The dimension correlation is

$$d_c = \lim_{r \to 0} \frac{\ln[C(r)]}{\ln\ r}. \tag{10}$$

Mañé [22] showed that the minimum number of state variables (here $2N$) required for modelling the system is given by $d_c \leqslant 2N \leqslant 2d_c + 2$. This is clearly the lower bound for the system dimension; in actual problems the number of degrees of freedom should be larger than the minimum in order to circumvent problems of convergence of the series adopted in expanding the displacement field.

Note that the choice of the delay time and the embedding dimension M is not trivial. In Ref. [24] the delay time is chosen in correspondence of the first zero of the autocorrelation function of the initial time series. On the other hand, Lai and Lerner [28] proved that, if the delay time is too large, an increasing of delay time can lead to wrong results as M increases. Lai and Lerner controlled the goodness of the delay time by looking at the linear region in the diagram ($\log C(r)$, $\log(r)$), and found that the range of the linear scaling region depends on both delay time and M, more sensitively on delay time. Once the correct delay time is chosen the correlation dimension is estimated from the slope of the ($\log C(r)$, $\log(r)$) curve, in the linear scaling region. The estimate is repeated for different values of the embedding dimension M, and the correct correlation dimension is obtained when saturation is reached, i.e., when the correlation dimension reaches a plateau versus M.

4.3. Lyapunov exponent

The evaluation of the correlation dimension is a powerful tool to evaluate both the system dimensionality and the chaoticity. Indeed, when the correlation dimension is not an integer, the dynamics evolves on a fractal set, i.e., one can observe chaotic evolutions.

However, in some cases evaluation of the correlation dimension is impossible, for example in the case of highly polluted data or high-dimensional chaos. In these cases one can evaluate the evolution properties by means of the Lyapunov exponents.

In the present work the maximum Lyapunov exponent is evaluated using an algorithm based on the work of Rosenstein et al. [32]. Consider the vector $\mathbf{v}_i$ on the embedding space; for $i = n'$ the system trajectory is close to a previously visited state n, i.e., $\mathbf{v}_{n'}$ is close to $\mathbf{v}_n$; the distance of these vectors is $\Delta_0 = \mathbf{v}_n - \mathbf{v}_{n'}$. Such a distance can be thought as a small perturbation of initial conditions, therefore one can follow the time evolution of the distance between two trajectories by writing: $\Delta_r = \mathbf{v}_{n+r} - \mathbf{v}_{n'+r}$; if $|\Delta_r| \approx |\Delta_0| \mathrm{e}^{\lambda t}$ than λ is the maximum Lyapunov exponent. Details of the algorithm can be found in Ref. [27]. The estimation of λt is given by

$$S(\varepsilon, m, t) = \left\langle \ln\left(\frac{\sum_{\mathbf{v}_{n'} \in \mathscr{U}_n} |w_{n+l} - w_{n'+l}|}{|\mathscr{U}_n|} \right) \right\rangle_n, \tag{11}$$

where m is the embedding dimension, and $\langle \cdot \rangle$ indicates average over a certain interval of data. The slope of S gives the maximum Lyapunov exponent with a good accuracy, if the straight region is found for several values of the perturbation and the embedding dimension.

4.4. Filtering

In the present work both numerical and experimental data are processed; in particular, the latter are highly polluted because the Laser measures the distance of the belt mid-span and the Laser beam reflects on a moving surface.

Here several filtering methods have been tested: average, median average, low pass filters; these classical methods did not gave satisfactory results. Therefore a non-linear noise reduction method [25] has been used; this method performs an averaging on the embedding vector $\mathbf{v}_i = \{w_{i-k}, ..., w_{i+l}\}$ having a unitary delay. For each embedding vector an average is performed by finding all vectors close to $\mathbf{v}_i$, i.e., by selecting a set $\mathscr{U}_i^\varepsilon$ of all neighbors of w_i that respect the condition: $\sup\{|w_{j-k} - w_{i-k}|, ..., |w_{j+l} - w_{i+l}|\} < \varepsilon$; the averaged sample is

$$w_i^{\text{corr}} = \frac{\sum_{\mathscr{U}_i^\varepsilon} w_i}{|\mathscr{U}_i^\varepsilon|}. \tag{12}$$

The practical implementation of this procedure is described in Ref. [25].

This non-linear filtering method is particularly efficient when data are highly polluted (more than 1% noise); conversely when small amount of noise is present it is not able to filter accurately and other methods should be used. Therefore, in the present work the present filter has been used, after several tests, because our experimental data present a large amount of noise.

5. Analysis of regular and chaotic motion

5.1. Hamiltonian dynamics

The first series of tests are performed on the model used in Ref. [16], which corresponds to Eq. (6) without excitation and damping. The test case considered in Ref. [16] is as follows: $L = 0.2\,\text{m}$, $A = 10^{-5}\,\text{m}^2$, $I = 2.08 \times 10^{-13}\,\text{m}^4$, $E = 2.1 \times 10^{11}\,\text{N/m}^2$, $\rho = 7600\,\text{kg/m}^3$, $P = 100\,\text{N}$; the corresponding non-dimensional quantities are $v_f = 0.104$, $v_T = 145$. The first three critical speeds are: $v^{(1)} = 1.05202$, $v^{(2)} = 1.19457$, $v^{(3)} = 1.40027$. A homoclinic orbit was discovered in Ref. [16] for $v \in (v^{(1)}, v^{(2)})$, and chaotic motion was found for $v > v^{(2)}$.

The first analysis is performed in the supercritical speed range, $v = 1.1$; an infinitesimal initial perturbation is given: $q_1(0) = 10^{-4}$, $q_i(0) = 0$, $i = 2, \ldots, N$ and $\dot{q}_i = 0$, $i = 1, \ldots, N$; $N = 12$. In Fig. 2a, the time history of $q_1(t)$ is shown, together with the Hamiltonian function $H(\mathbf{q}(t))$. The dynamics are extremely slow and periodic, the period depends essentially on the initial condition, and approaches infinity when the initial perturbation tends to zero; this property of homoclinic orbits is well known in the literature. The analysis is performed by means of an adaptive step-size Runge–Kutta routine, and the results are sampled with $\Delta t = 0.5$, which allow more than 20 samples per period. By analyzing the correlation function of the time history, the first zero is found for $11\Delta t$; therefore the following delay $d = 11$ is assumed for the embedding space. The reconstructed orbit is shown within Fig. 2a, which shows that the topologic characteristics of the homoclinic orbit are preserved (see Ref. [16]). In Fig. 2b the slope of the correlation integral, which gives the correlation dimension, is shown versus the scale length for various embedding

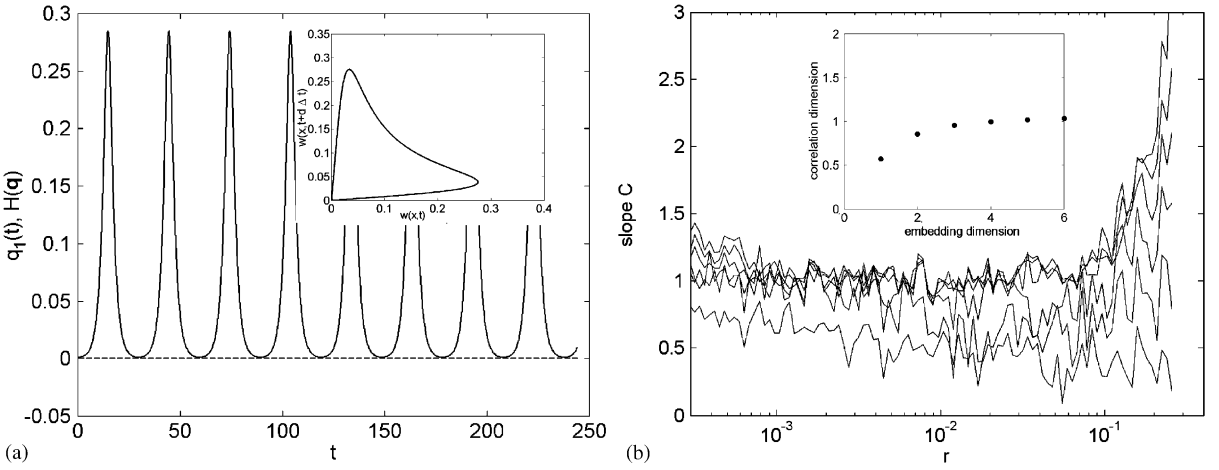

Fig. 2. Homoclinic orbit. (a) Time history '–', Hamiltonian function '- -' and embedding phase space $d = 11$, $\Delta t = 0.5$ (picture included); (b) slope of the correlation integral versus scaling dimension and correlation dimension versus embedding dimension (picture included).

dimensions. Fig. 2b shows that a large plateau is obtained, two decades; moreover, the picture included in Fig. 2b shows that the convergence to $d_c = 1$ is reached. Indeed, the homoclinic orbit is a one-dimensional set. The maximum Lyapunov exponent, evaluated from the time series, i.e., simulating an experimental measurement, for this system is zero.

A similar analysis has been performed for, $v = 1.3$, a small initial perturbation is given as $q_1(0) = 0.01$, $q_i(0) = 0$, $i = 2, \ldots, N$ and $\dot{q}_i = 0$, $i = 1, \ldots, N$ with $N = 12$. In Fig. 3a, the time history of $q_1(t)$ is shown together with the Hamiltonian function $H(\mathbf{q}(t))$. The dynamics present an intermittent chaotic behavior; the Hamiltonian function is almost constant, proving sufficient accuracy of the numerical algorithm in this particular condition. The spectrum is almost continuous (picture included in Fig. 3a) and no fundamental frequency can be identified. In this case the correlation dimension has not been computed; indeed, long and short time scales are present and the correlation integral slope does not give a clear measure of the correlation dimension. This is probably due to the intermittency and the transient chaotic behavior observed in this condition. In Fig. 3b the slope of the function S gives an estimate of the maximum Lyapunov exponent; the best estimation is obtained when the function S becomes straight; in Fig. 3b, a thick straight line is added to indicate the average slope. In Fig. 3b several lines are present; indeed, the estimation is performed by selecting various embedding dimensions and perturbations of the initial condition. In this case a positive slope is found, indicating a chaotic dynamics, and the estimation of the maximum Lyapunov exponent is: $\lambda \approx 1.5$.

5.2. *Chaotic dynamics: external forcing and damping*

Chaotic dynamics has been extensively analyzed in Ref. [17]; in that study the travelling beam analyzed in Section 5.1 (Ref. [17]) was forced with a harmonic external point excitation $\tilde{f}(x, t)$, and a viscous damping was introduced in order to consider structural dissipation, corresponding to a

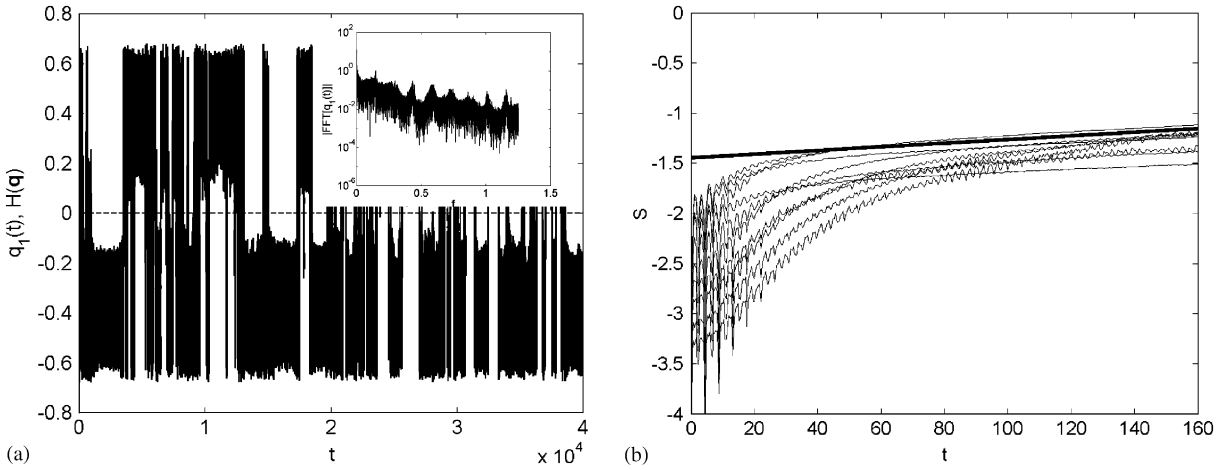

Fig. 3. Hamiltonian chaos. (a) Time history '–', Hamiltonian function '- -' and spectrum (picture included); (b) estimation of the maximum Lyapunov exponent.

2% modal damping. Interesting results were found when the axial speed was larger than the critical one. In Fig. 4 the slope of the correlation integral versus scaling dimension, the correlation dimension versus embedding dimension, converging to $d_c \cong 1.6$, and the Poincaré section of the flow are shown for: excitation amplitude and frequency $f = 0.54$, $\omega = 0.567$, axial speed $v = 1.1$. In Ref. [16] a homoclinic orbit was found for the free undamped problem, see previous section; for the same axial speed the introduction of damping and a suitable harmonic point excitation showed that the system responded chaotically. However, the question whether the dynamics is governed by a low-dimensional Duffing-type oscillator has no answer. Because of the presence of complex modes, the physical problem cannot be represented through a single real ordinary differential equation; in Ref. [17] it was shown that a low-dimensional system is not able to reproduce this chaotic behavior, even though the analysis was connected with the series used in expanding the displacement field. In the present study one can find an answer to the previous question: the correlation dimension is 1.6; see Fig. 4. The result of the present analysis is that the chaotic dynamics is low dimensional, it is developed on a fractal attractor and a single degree of freedom system could be able to capture the essential characteristics of the system response. It is interesting to note that in Ref. [26] $d_c = 1.6$ and 1.7 is obtained from experimental data regarding a special set-up, which simulated a chaotic Duffing-type oscillator having one and two frequency excitation, respectively. This confirms the topological similarity of the scenario obtained in Ref. [17] with that of a Duffing oscillator; and is a further confirmation of the universal properties of Chaos.

5.3. *Parametric resonance: theory and experiments*

In this section the dynamic behavior of a flat belt is analyzed. The driven pulley presents an eccentricity, which gives a direct (seismic) and a parametric (tension fluctuation) excitation. The belt cross-section area is $A = (2.5 \times 10^{-3}) \times (22.9 \times 10^{-3})\,\mathrm{m}^2$ and the mass per unit length is

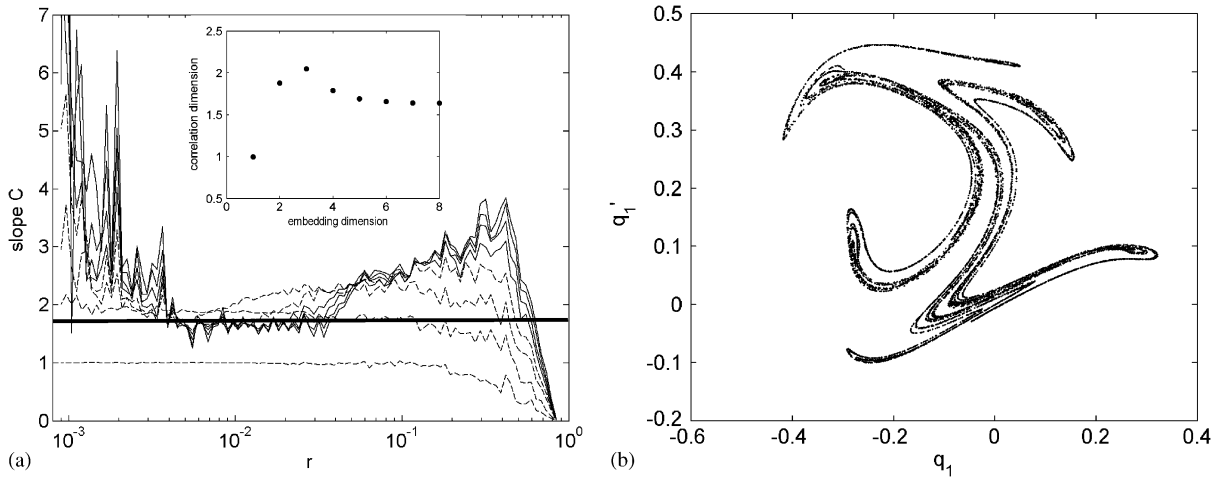

Fig. 4. Forced chaotic dynamics, damped axially moving beam: (a) slope of the correlation integral versus scaling dimension and correlation dimension versus embedding dimension (picture included), converging to $d \cong 1.6$; (b) Poincaré section. Excitation: amplitude $f = 0.54$, frequency $\omega = 0.567$, axial speed $v = 1.1$.

$\rho \times A = 0.0626\,\mathrm{kg/m}$ (synthetic reinforced rubber). The radius of the driven and driver pulleys is $R = 0.1\,\mathrm{m}$, and the tightener radius is 0.026 m; the distance between the pulley axes is $l = 1.01\,\mathrm{m}$. For this problem several analytical and numerical models were developed in the past, see e.g. Refs. [6,18]. In particular, both low- and high-dimensional models showed a good agreement with experiments; even though both low- and high-dimensional methods were able to capture the main phenomena related to the parametric instability, some complex dynamics were captured with high-dimensional models only.

Here experimental data used in Ref. [18] are reanalyzed in order to obtain the actual statistical dimension of the attractor.

The first case corresponds to the typical one-half sub-harmonic response arising from the principal parametric instability. This problem can be described with good accuracy through a 1-d.o.f. complex system, obtained using a single complex mode Galekin projection [6]. Indeed, in Fig. 5a the correlation dimension shows that a clear saturation is encountered at $d_c = 1$, the slope of the correlation integral shows a large flat region, which assures that the statistical evaluation is accurate. This result justifies completely the 1-d.o.f. model presented in Ref. [6]. In Fig. 5b the phase trajectory obtained through the use of the first two embedding coordinates is shown; this reconstruction is performed on the measured data and clearly presents a strong pollution. In this case the classical filtering techniques, e.g., moving average, were not able to remove noise. After the non-linear filtering the phase trajectory (Fig. 5c) appears quite regular and cleaned. The correlation dimension estimation converged on filtered data only.

In Ref. [18] interesting complex dynamics were experimentally observed, and a high-dimensional numerical model was used to reproduce these data. In Fig. 6 a one-third sub-harmonic response is analyzed; also in this case the attractor is almost one-dimensional, even though the data pollution was not removed completely and the saturation is not completely satisfactory.

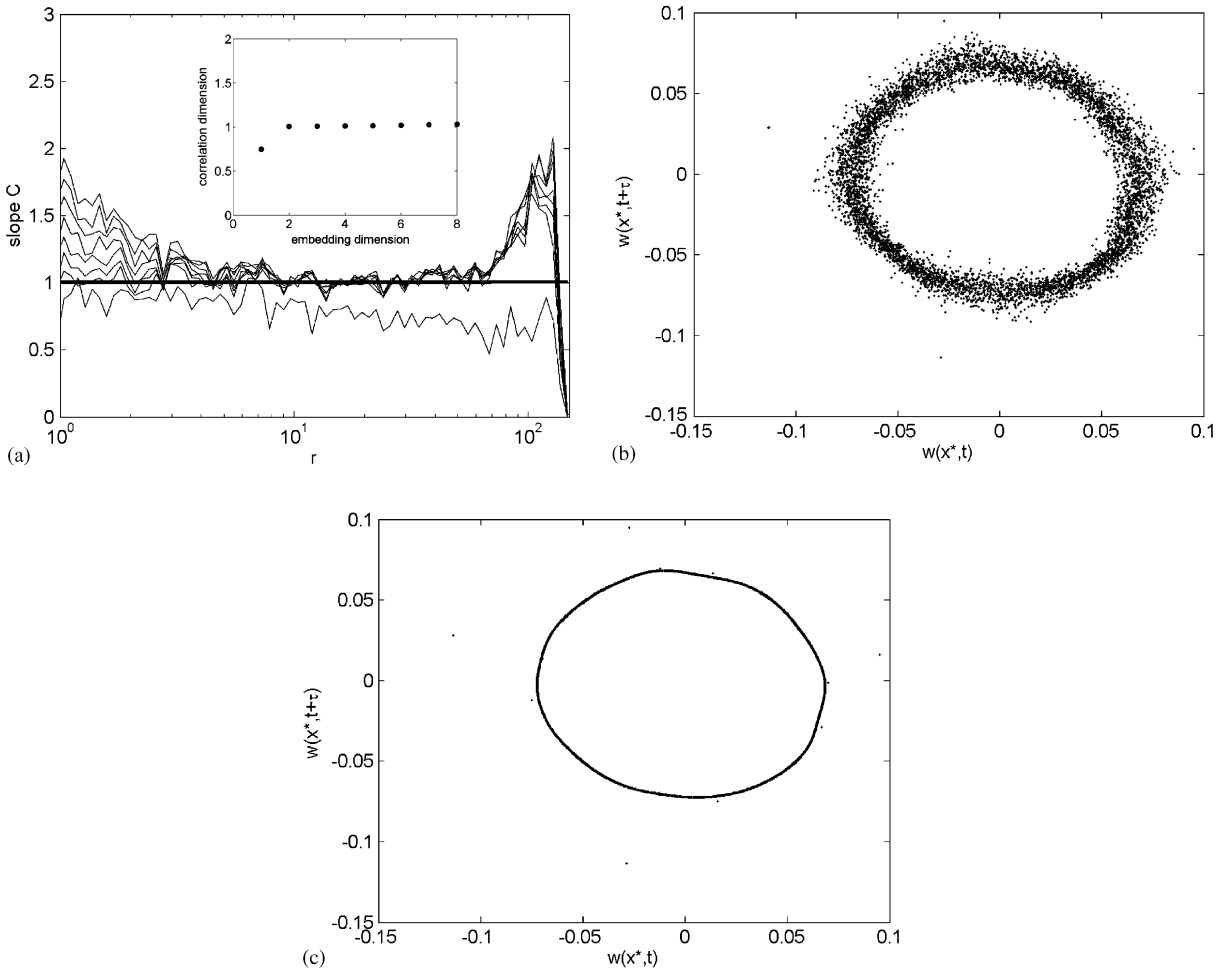

Fig. 5. Parametric resonance: one-half sub-harmonic response. Experimental results for: eccentricity 3.2×10^{-3} m, excitation frequency 40 Hz. (a) Correlation integral and correlation dimension (picture included); (b) phase trajectory for measured data; (c) phase trajectory for filtered data.

In Ref. [18] quasi-periodic responses were experimentally observed and the numerical model was able to reproduce similar behaviors in some cases. Unfortunately, the experimental data corresponding to those quasi-periodic motions reproduced numerically were too polluted and the data analysis gave no saturation. However, a qualitative analysis can be performed; in Fig. 7a the correlation integral slope is shown, even though the pollution does not allow a clear saturation of the dimension. From this picture one can argue that probably the dynamics is developed on a two-dimensional set. The estimation of the maximum Lyapunov exponent shows highly oscillating behavior, due to the noise (Fig. 7b); however, a flat region is clearly visible, indicating that the maximum Lyapunov exponent is almost zero. Figs. 7c,d show the embedding phase trajectories before and after filtering. In the original data the noise completely obscured the flow structure; the filtering in this case was not able to remove the noise completely, but clearly evidences the structure of the dynamics. Numerical simulations, performed at different excitation frequency,

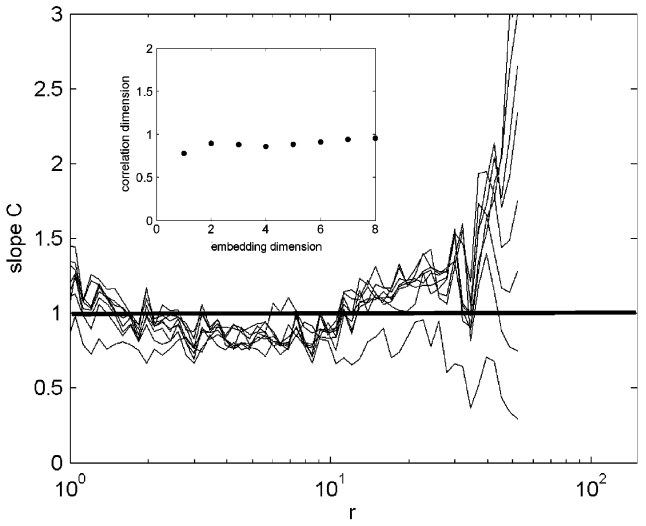

Fig. 6. Parametric resonance: one-third sub-harmonic response. Experimental results for: eccentricity 3.2×10^{-3} m, excitation frequency 40.2 Hz; correlation integral and correlation dimension (picture included).

show a similar amplitude modulation; in this case the dimension evaluation is quite easy and show a saturation on a two-dimensional set; the results are not reported for the sake of brevity.

This qualitative analysis clearly indicates that a strongly reduced order model [6] cannot simulate amplitude modulations, and fully justifies the development of the high-dimensional model of Ref. [18]. However, such analysis encourages those who attempt to develope a low-dimensional, 2-d.o.f. model at least, enhancing for example the theory developed in Ref. [6].

6. Conclusions

The dynamic properties of axially moving systems are analyzed in order to explain complex dynamic behaviors, which were observed in experimental and numerical investigations. Both Hamiltonian and dissipative systems have been investigated, by using non-linear time series analysis.

Taking advantage of the Hamiltonian formulation it is proven that the classical governing equations of axially moving systems, reduced to ODE by means of the Galerkin method, preserve the Hamiltonian properties.

By using several non-linear time series techniques, correlation dimension and Lyapunov exponents have been evaluated. The analysis of time series proves that, for the dissipative cases, a low-dimensional model is able to capture the essential dynamics. In particular, sub-harmonic responses of dissipative axially moving systems evolve on one-dimensional attractors, and quasi-periodic motions evolve on two-dimensional attractors; conversely, chaotic responses belong to a low-dimensional fractal attractor. In the case of Hamiltonian dynamics, the time series analysis was applied to the evaluation of the maximum Lyapunov exponent. A positive exponent was found which confirms the conjectures made in the past about the sensitivity to initial conditions.

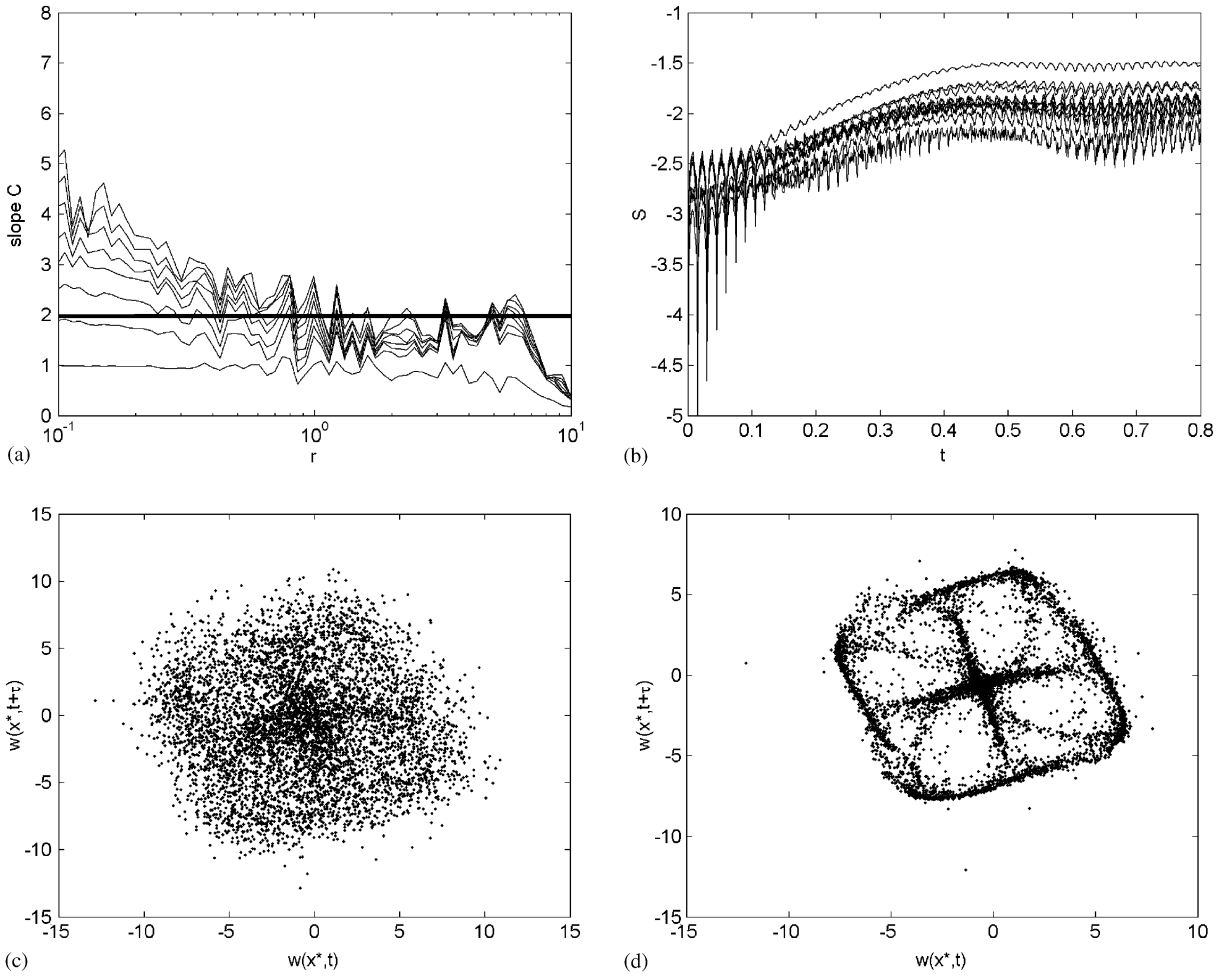

Fig. 7. Parametric resonance: quasi-periodic response. Experimental results for: eccentricity 1.25×10^{-3} m, excitation frequency 17 Hz. (a) Correlation integral; (b) estimation of the maximum Lyapunov exponent; (c) phase trajectory for measured data; (d) phase trajectory for filtered data.

Finally, in the analysis of experimental data, a fundamental improvement in the data processing must be addressed to the non-linear filtering methods based on embedding techniques. These new filtering methods are very promising tools when experimentalists are concerned with highly polluted data.

Appendix

Let us now eliminate direct excitations from Eq. (4) and, for the sake of simplicity consider fixed ends, i.e., an infinitely rigid spring in the model presented in Fig. 1a. With these assumptions the matrix **K** becomes a symmetric constant matrix. Eq. (6) can be obtained from the Lagrangian

equations

$$\frac{\mathrm{d}}{\mathrm{d}t}\left(\frac{\partial L}{\partial \dot{\mathbf{q}}}\right) - \left(\frac{\partial L}{\partial \mathbf{q}}\right) = \mathbf{0}, \tag{A.1}$$

where the Lagrangian function is

$$L = T - U = \tfrac{1}{2}\dot{\mathbf{q}}^{\mathrm{T}}\dot{\mathbf{q}} - \tfrac{1}{2}\mathbf{q}^{\mathrm{T}}\mathbf{C}\dot{\mathbf{q}} - U(\mathbf{q}). \tag{A.2}$$

Let us introduce the matrix $\mathbf{C}_1 = \mathbf{C}/2$ and introduce the generalized momenta

$$\mathbf{p} = \frac{\partial L}{\partial \dot{\mathbf{q}}} = \dot{\mathbf{q}} + \mathbf{C}_1\mathbf{q}. \tag{A.3}$$

A first integral of motion can be found through the Legendre transformation, which gives the Hamiltonian function of the system:

$$H(\mathbf{p}, \mathbf{q}) = \mathbf{p}^{\mathrm{T}}\dot{\mathbf{q}} - L = \text{const.} \tag{A.4}$$

It is well known that the Hamiltonian H is an invariant of the system, i.e., H is independent of t, and its value depends only on the initial conditions. For this specific problem, Eq. (A.4) gives

$$H = \mathbf{p}^{\mathrm{T}}\dot{\mathbf{q}} - \tfrac{1}{2}\dot{\mathbf{q}}^{\mathrm{T}}\dot{\mathbf{q}} + \mathbf{q}^{\mathrm{T}}\mathbf{C}_1\dot{\mathbf{q}} + U(\mathbf{q}). \tag{A.5}$$

After some algebra, one finds

$$H(\mathbf{p}, \mathbf{q}) = \tfrac{1}{2}\mathbf{p}^{\mathrm{T}}\mathbf{p} - \mathbf{p}^{\mathrm{T}}\mathbf{C}_1\mathbf{q} - \tfrac{1}{2}\mathbf{q}^{\mathrm{T}}\mathbf{C}_1^2\mathbf{q} + U(\mathbf{q}). \tag{A.6}$$

The Hamiltonian form of the governing equations becomes

$$\dot{\mathbf{p}} = -\frac{\partial H}{\partial \mathbf{q}}, \quad \dot{\mathbf{q}} = \frac{\partial H}{\partial \mathbf{p}} \tag{A.7}$$

which yield

$$\begin{aligned} \dot{\mathbf{p}} &= -\mathbf{C}_1\mathbf{p} + \mathbf{C}_1^2\mathbf{q} - \frac{\partial U}{\partial \mathbf{q}}, \\ \dot{\mathbf{q}} &= \mathbf{p} - \mathbf{C}_1\mathbf{q}. \end{aligned} \tag{A.8}$$

It can be easily proven that Eq. (A.8) can be transformed into the initial equations through the definition of generalized momenta (A.7).

Eq. (A.8) can be used to reduce the system dimension by one. However, Eq. (A.6) can be rewritten in terms of the natural coordinates:

$$H(\dot{\mathbf{q}}, \mathbf{q}) = \tfrac{1}{2}\dot{\mathbf{q}}^{\mathrm{T}}\dot{\mathbf{q}} + U(\mathbf{q}). \tag{A.9}$$

In the case of axially moving beams without external excitations, Eq. (6) reads

$$\begin{aligned} &\ddot{q}_n - \sum_{k=1, k\neq n}^{N} k\left[\frac{(-1)^{n+k}-1}{n+k} + \frac{(-1)^{n-k}-1}{n-k}\right]\dot{q}_k + \left[v_f^2 n^4\pi^4 - \left(v^2-1\right)n^2\pi^2\right] q_n \\ &\quad + \frac{v_T^2 n^2\pi^4}{4} q_n \sum_{k=1}^{N} k^2 q_k^2 = 0 \end{aligned} \tag{A.10}$$

and the elastic potential energy can be written as

$$U(\mathbf{q}) = \frac{1}{2}\sum_{n=1}^{N} K_n q_n^2 + \frac{1}{4}\sum_{n=1}^{N}\sum_{k=1}^{N} \beta_{nk} q_n^2 q_k^2, \tag{A.11}$$

where $K_n = v_f^2 n^4\pi^4 - (v^2 - 1)n^2\pi^2$ and $\beta_{nk} = v_T^2 n^2 k^2 \pi^4/4$.

References

[1] H. Ashley, G. Haviland, Bending vibrations of a pipe line containing flowing fluid, *Journal of Applied Mechanics* 17 (1950) 229–232.

[2] R.D. Swope, W.F. Ames, Vibrations of a moving threadline, *Journal of Franklin Institute* 275 (1963) 36–55.

[3] C.D. Mote Jr., On the non-linear oscillation of an axially moving string, *Journal of Applied Mechanics* 33 (1966) 463–464.

[4] S. Naguleswaran, J.H. Williams, Lateral vibration of band-saw blades, pulley belts and the like, *International Journal of Mechanical Science* 10 (1968) 239–250.

[5] A.M. Mockensturm, N.C. Perkins, A.G. Ulsoy, Stability and limit cycles of parametrically excited, axially moving strings, *Journal of Vibration and Acoustics* 118 (1996) 346–351.

[6] F. Pellicano, A. Fregolent, A. Bertuzzi, F. Vestroni, Primary and parametric non-linear resonances of a power transmission belt: experimental and theoretical analysis, *Journal of Sound and Vibration* 244 (4) (2001) 669–684.

[7] L.Y. Shih, Three-dimensional non-linear vibration of a traveling string, *International Journal of Non-Linear Mechanics* 6 (1971) 427–434.

[8] W.F. Ames, S.Y. Lee, J.N. Zaiser, Non-linear vibration of a travelling threadline, *International Journal of Non-Linear Mechanics* 3 (1968) 449–469.

[9] A. Simpson, Transverse modes and frequencies of beams translating between fixed end supports, *Journal of Mechanical Engineering Science* 15 (1973) 159–164.

[10] J.A. Wickert, C.D. Mote Jr., Classical vibration analysis of axially moving continua, *Journal of Applied Mechanics* 57 (1990) 738–744.

[11] P.J. Holmes, Pipes supported at both ends cannot flutter, *Journal of Applied Mechanics* 45 (1978) 619–622.

[12] M.P. Païdoussis, F.C. Moon, Non-linear and chaotic fluidelastic vibrations of a flexible pipe conveying fluid, *Journal of Fluids and Structures* 2 (1988) 567–591.

[13] J.A. Wickert, Non-linear vibration of a travelling tensioned beam, *International Journal of Non-Linear Mechanics* 27 (1992) 503–517.

[14] S.J. Hwang, N.C. Perkins, Supercritical stability of an axially moving beam—part I: model and equilibrium analysis, *Journal of Sound and Vibration* 154 (3) (1992) 381–396.

[15] S.J. Hwang, N.C. Perkins, Supercritical stability of an axially moving beam—part II: Vibration and stability analyses, *Journal of Sound and Vibration* 154 (3) (1992) 397–409.

[16] F. Pellicano, F. Vestroni, Non-linear dynamics and bifurcations of an axially moving beam, *Journal of Vibration and Acoustics* 122 (2000) 21–30.

[17] F. Pellicano, F. Vestroni, Complex dynamics in high speed axially moving systems, *Journal of Sound and Vibration* 258 (1) (2002) 31–44.

[18] F. Pellicano, G. Catellani, A. Fregolent, Parametric instability of belts: theory and experiments, *Computers & Structures* 82 (1) (2004) 81–91.

[19] C.C. Lin, Stability and vibration characteristics of axially moving plates, *International Journal of Solids and Structures* 34 (24) (1997) 3179–3190.

[20] P. Grassberger, I. Procaccia, Measuring the strangeness of strange attractors, *Physica D* 9 (1983) 189–208.

[21] P. Grassberger, I. Procaccia, Characterization of strange attractors, *Physical Review Letters* 50 (1983) 346–349.

[22] R. Mañé, On the dimension of compact invariant sets of certain non-linear maps, in:D. Rand, L.S. Young (Eds.), *Dynamical Systems and Turbolence, Lecture Notes in Mathematics*, Vol. 898, Springer, Berlin, 1981, pp. 230–242.

[23] J.P. Eckmann, D. Ruelle, Ergodic theory of chaos and strange attractors, *Reviews Modern Physics* 57 (1985) 617–656.
[24] A. Provenzale, L.A. Smith, R. Vio, G. Murante, Distinguishing between low-dimensional dynamics and randomness in measured time series, *Physica D* 58 (1992) 31–49.
[25] T. Schreiber, Extremely simple non-linear noise reduction method, *Physics Review E* 47 (1993) 2401–2404.
[26] L.N. Virgin, *Introduction to Experimental Non-linear Dynamics*, Cambridge University Press, Cambridge, MA, 2000.
[27] H. Kantz, A robust method to estimate the maximal Lyapunov exponent of a time series, *Physics Letters A* 185 (1994) 77–87.
[28] Y.C. Lai, D. Lerner, Effective scaling regime for computing the correlation dimension from chaotic time series, *Physica D* 115 (1998) 1–18.
[29] R. Hegger, H. Kantz, T. Schreiber, Practical implementation of non-linear time series methods: the TISEAN package, *CHAOS* 9 (1999) 413.
[30] A.L. Thurman, C.D. Mote Jr., Free, periodic, non-linear oscillation of an axially moving strip, *Journal of Applied Mechanics* 36 (1969) 83–91.
[31] F. Takens, *Detecting Strange Attractors in Turbulence*, Lecture Notes in Mathematics, Vol. 898, Springer, New York, 1981.
[32] M.T. Rosenstein, J.J. Collins, C.J. De Luca, A practical method for calculating largest Lyapunov exponents from small data sets, *Physica D* 65 (1993) 117.
[33] H. Kantz, T. Schreiber, *Non-linear Time Series Analysis*, Cambridge University Press, Cambridge, MA, 1997.